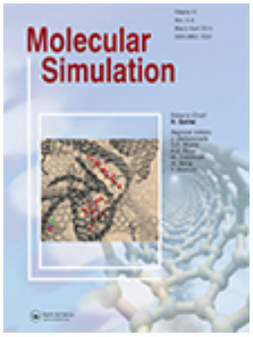

Molecular Simulation

ISSN: 0892-7022 (Print) 1029-0435 (Online) Journal homepage: https://www.tandfonline.com/loi/gmos20

Molecular simulation of shale gas adsorption and diffusion in inorganic nanopores

Aman Sharma, Sadanandam Namsani & Jayant K. Singh

To cite this article: Aman Sharma, Sadanandam Namsani & Jayant K. Singh (2015) Molecular simulation of shale gas adsorption and diffusion in inorganic nanopores, Molecular Simulation, 41:5-6, 414-422, DOI: 10.1080/08927022.2014.968850

To link to this article: https://doi.org/10.1080/08927022.2014.968850

Molecular Simulation, 2015
Vol. 41, Nos. 5–6, 414–422, http://dx.doi.org/10.1080/08927022.2014.968850

Taylor & Francis
Taylor & Francis Group

CONFINED FLUIDS

Molecular simulation of shale gas adsorption and diffusion in inorganic nanopores

Aman Sharma, Sadanandam Namsani and Jayant K. Singh*

Department of Chemical Engineering, Indian Institute of Technology Kanpur, Kanpur 208016, India

(*Received 23 June 2014; final version received 15 September 2014*)

We studied the structural and dynamical properties of methane and ethane in montmorillonite (MMT) slit pore of sizes 10, 20 and 30 Å using grand canonical Monte Carlo and classical molecular dynamics (MD) simulations. The isotherm, at 298.15 K, is generated for pressures up to 60 bar. The molecules preferentially adsorb at the surface as indicated by the density profile. In case of methane, we observe only a single layer, at the pore wall, whose density increases with increasing pressure. However, ethane also displays a second layer, though of low density in case of pore widths 20 and 30 Å. In-plane self-diffusion coefficient, $D_{||}$, of methane and ethane is of the order of 10^{-6} m^2/s. At low pressure, $D_{||}$ increases significantly with the pore size. However, $D_{||}$ decreases rapidly with increasing pressure. Furthermore, the effect of pore size on $D_{||}$ diminishes at high pressure. Ideal adsorbed solution theory is used to understand the adsorption behaviour of the binary mixture of methane (80%) and ethane (20%) at 298.15 K. Furthermore, we calculate the selectivity of the gases at various pressures of the mixture, and found high selectivity for ethane in MMT pores. However, selectivity of ethane decreases with increase in pressure or pore size.

Keywords: montmorillonite; methane; ethane; shale gas; GCMC

1. Introduction

Due to rising prices of crude oil and natural gas, the focus has shifted towards unconventional sources of energy. Shale gas is one of the most important candidates among them. Unconventional reservoirs, particularly shale gas reservoirs, present some distinctive challenges to the petroleum industry. Notwithstanding the requirement of large scale production of shale gas throughout the world, the thermodynamics properties of shale gas is still far from being clearly understood.[1]

One of the major challenges in the shale gas production is the estimation of gas content in the reservoir.[2] It is stored in shales as free gas in tiny spaces in rocks or adsorbed gas attached to organic matter and clays.[3] Montgomery et al. [4] showed that the adsorbed gas amounts to more than half of the total gas content. Shale comprises inorganic and organic materials.[5] Kerogen forms the major constituent of the organic material and is insoluble in organic solvents.[6,7] Few studies suggest that bulk of the sorbed gas is contained in organic matter, and knowing the total organic content of the shale is enough to estimate the adsorbed gas.[8–10] On the other hand, other studies have shown that the amount of sorbed gas is comparable in clays and organic matter.[11–13] Thus, the role of inorganic materials, particularly clays with microporous structure, in the adsorption of gas cannot be neglected.[14–16] Therefore, estimating the gas content in clays is as important as in organic matter. Cheng et al. [17] showed that clays with micropore in the range of 10–20 Å provide large surface areas and serve as the adsorption sites for gases. Yuan and coworkers [18] experimentally characterised the shale materials, from the Sichuan Basin of China, and obtained micro pores in the range of few nanometres.

Numerous studies on molecular simulations for water adsorption, swelling and hydration behaviour of clays have been reported.[19–22] However, gas adsorption has not been extensively studied. Though carbonaceous materials have been widely used for molecular simulations of gas sorption,[23–28] chemical heterogeneity is not much prevalent unlike in clays. Some studies have shown that chemical heterogeneity of the clay pores plays a key role in gas sorption under confinement.[29–32] For example, Yang and Zhang [28] performed MD studies to understand diffusion behaviour of dense CO_2 in clay slit pores. Botan et al. [33] studied thermodynamical, structural and transport properties of CO_2 in montmorillonite (MMT) using grand canonical Monte Carlo (GCMC) and MD simulations. Cygan et al. [34] studied carbon intercalation mechanism in MMT clays and the effect of molecular flexibility on diffusion rate of CO_2 in water using MD studies. However, adsorption and transport properties of major components of shale gas in clay materials are yet to be investigated.

Composition of the shale gas varies depending on the location of the shale reservoirs. The gas contains methane (70–90%), as the major component, along with other hydrocarbons, such as ethane, propane, butane (0–20%) and gases such as carbon dioxide and nitrogen (0–5%).[1]

*Corresponding author. Email: jayantks@iitk.ac.in

Table 1. Composition of wells for Marcellus and Barnett shale [59].

Components	Marcellus well (%)	Barnett well (%)
Methane	79.4	81.2
Ethane	16.1	11.8
Propane	4.0	5.2
Carbon dioxide	0.1	0.3
Nitrogen	0.4	1.5

Table 1 lists the composition of the gas from Marcellus and Barnett shale in the USA. The aim of this work is to understand the key reservoir parameters, such as sorption capacity and transport coefficients, which can provide greater insights into the production of shale gas, using molecular simulations. In this work, we have taken methane and ethane as the only constituents of the shale gas with the mole fraction of methane as 80% and ethane as 20%. We have considered Monte Carlo simulations in grand canonical (μVT) ensemble as it is a suitable choice for investigating gas adsorption in porous materials. [35,36] Subsequently, ideal adsorbed solution theory (IAST) was used to obtain binary mixture isotherms using pure component isotherms. Furthermore, MD simulations were performed in order to investigate the diffusion coefficients of methane and ethane molecules in clay pores. The rest of the article is organised as follows. In Section 2 we describe the models and methodology employed in this work. Section 3 presents the results and discussions followed by the conclusion in Section 4.

2. Models and methodology

In general, clays comprise large number of particles arranged in piles of sheets.[37] To model the clay, we have taken the MMT structure which is made up of two tetrahedral sheets fused with an octahedral sheet.[38] In this work, neutral MMT structure without any interlayer ions is considered.[39] The unit cell of MMT clay was taken from Skipper et al. [40]. Several studies on molecular simulations of water and hydrate formation in clay minerals have used the same unit cell, affirming its wide applicability.[22,39,41–43] Methane molecule was modelled as a single-site Lennard-Jones particle, and ethane molecule was modelled as a two-site Lennard-Jones particle with a fixed bond between them.

2.1 Models

We use MMT, which is a dioctahedral 2:1 clay mineral, without any cation exchange as the adsorbent. Its unit cell formula is $Si_8Al_4O_{20}(OH)_4$ with unit cell parameters as $a = 5.24$ Å, $b = 9.14$ Å, $c = 6.56$ Å. There are 32 clay unit cells in our simulation cell which results in a clay sheet of 42.24 Å × 36.56 Å with a thickness of 6.56 Å separated by a distance (depending on the pore size) to represent a slit pore. We have considered two layers in our clay model as also adopted for the study of water adsorption in MMT. [39] The positions of the atoms in MMT were taken from Skipper et al. [40].

The potential model used for ethane was taken from Jorgensen et al. [44], and TraPPE force field [45] was employed for methane. The united atom model was used for both methane and ethane with the CH_3–CH_3 bond, in case of ethane, considered as rigid with a bond length of 1.839 Å.[46] Non-bonded site–site interactions are described by the Lennard-Jones 12-6 potential,

$$u(r_{ij}) = 4\varepsilon_{ij}\left[\left(\frac{\sigma_{ij}}{r_{ij}}\right)^{12} - \left(\frac{\sigma_{ij}}{r_{ij}}\right)^{6}\right], \quad (1)$$

where r_{ij}, ε_{ij} and σ_{ij} are the distance between sites i and j of two molecules, Lennard-Jones well depth and distance at which the inter-site potential is zero, respectively. The Lorentz–Berthelot combining rules were used to calculate interactions between unlike atoms.

The DREIDING force field was used to describe the interaction parameters for atoms of MMT.[47] All the Lennard-Jones parameters are listed in Table 2. A cut-off radius of 10.7 Å was used for truncating Lennard-Jones interactions. To model the slit pore, periodic boundary conditions were used in two dimensions (along x and y) only.

2.2 Monte Carlo simulations

In this work, GCMC simulations were carried out to study the adsorption isotherms of methane and ethane in clay pores. The simulations were conducted in a grand canonical (μVT) ensemble where chemical potential (μ), volume (V) and temperature (T) are held constant, and number of particles (N) and energy (U) vary. The simulation cell is a cuboidal box with periodicity in the x and y directions only. The dimensions of the box are 42.24 Å in the x direction and 36.56 Å in the y direction. The length in the z direction depends on the size of the pore

Table 2. Lennard-Jones parameters of methane,[45] ethane[44] and MMT [47] atoms.

Atom	ε (K)	σ (Å)
Methane CH_4	148.0	3.73
Ethane CH_3	104.18	3.775
Clay		
Al	32.707	4.112
H	0	0
O	78.18	3.166
Si	47.803	3.951

which is defined as the distance between the inner walls of the two layers.

For each Monte Carlo cycle, the moves implemented were displacement of a randomly selected adsorbate molecule, random removal or insertion of an adsorbate molecule into the simulation box and random rotation of an adsorbate molecule (only for the case of ethane). The equilibrium and production runs consist of 0.1 and 0.5 million cycles, respectively. The system temperature was fixed at 298.15 K for all the simulations.

The Langmuir isotherm equation was used to fit the data generated from the simulations:

$$\frac{P_i}{q_i} = \frac{1}{Kq_m} + \frac{1}{q_m} P_i, \tag{2}$$

where P_i is the pressure and q_i (mmol/g) is the amount of gas adsorbed. Here K is constant of the Langmuir isotherm and q_m (mmol/g) is maximum adsorption capacity. To study the effect of density of the adsorbed phase (or pressure of the gas) on the diffusion of adsorbate in clay nanopores, we have used MD simulations using LAMMPS package.[48] All MD simulations were performed using the equilibrium configuration obtained from GCMC simulations. MD simulations were carried out using canonical (NVT) ensemble with a time step of 1 fs. Molecular configurations of the systems were stored for every 100 steps of the simulation. The generated configurations were used to calculate the self-diffusion coefficient and the density profiles of methane and ethane in MMT pores. To calculate the self-diffusion coefficient in the direction parallel to the pore walls, Einstein relation was employed:

$$D_{\|} = \frac{1}{4}\frac{d}{dt}\left\langle [r_x(t) - r_x(t_0)]^2 + \left[r_y(t) - r_y(t_0)\right]^2 \right\rangle, \tag{3}$$

where t is the simulation elapsed time and t_0 is the arbitrary starting point, and $\left\langle [r_x(t) - r_x(t_0)]^2 + \left[r_y(t) - r_y(t_0)\right]^2 \right\rangle$ is the mean square displacement along the plane of the pore. Plane self-diffusion coefficient, $D_{\|}$, of adsorbate was also calculated at different pressures for various MMT pore sizes.

2.3 Ideal adsorbed solution theory

The IAST [49] is a thermodynamic method used to predict the mixture isotherms using pure component adsorption isotherms. It is based on direct analogy between the Raoult's law in vapour–liquid and gas–adsorbate systems. It assumes that the adsorbed phase forms an ideal solution of the adsorbed components, which is a reasonable assumption for a binary mixture of methane and ethane.[50]

In this work, we have used the treatment of LeVan and Vermeulen [50] to obtain the binary isotherms for the adsorption of components which are given by the following expressions:

$$q_1 = \frac{\bar{q}P_1^*}{1 + P_1^* + P_2^*} + (q_{m,1} - q_{m,2}) \times \frac{P_1^* P_2^*}{\left(P_1^* + P_2^*\right)^2} \ln(1 + P_1^* + P_2^*), \tag{4}$$

$$q_2 = \frac{\bar{q}P_2^*}{1 + P_1^* + P_2^*} + (q_{m,2} - q_{m,1}) \times \frac{P_1^* P_2^*}{\left(P_1^* + P_2^*\right)^2} \ln(1 + P_1^* + P_2^*), \tag{5}$$

where P^* is a dimensionless parameter defined as $P_i^* = KP_i$, where K is constant in Langmuir isotherm equation, P_i is the partial pressure of component i in gas phase and $\overline{q}$ is the weighted monolayer capacity. q_1 and q_2 are quantity of gas adsorbed for components 1 and 2, respectively. Using the results from IAST, we calculate the selectivity of MMT for ethane relative to methane in methane–ethane binary mixture for different pore sizes. The selectivity is calculated using the following equation. [51]

$$\alpha_{1,2} = \frac{x_1/y_1}{x_2/y_2} = \frac{P_2^0}{P_1^0}, \tag{6}$$

where $\alpha_{1,2}$ is the selectivity of component 1 relative to component 2, $x_1$and x_2 are mole fractions of components 1 and 2 in the adsorbed phase, y_1 and y_2 are mole fractions of components 1 and 2 in the gas phase, and $P_1^0$and P_2^0 are vapour pressures of components 1 and 2 in the pure phase.

3. Results and discussion

3.1 Structural properties of methane and ethane in slit pore

Figure 1 presents the adsorption isotherms of methane for different pore sizes, using GCMC simulations. The total amount of methane adsorbed (q) increases with pressure, as expected. The amount of adsorption at low pressures is relatively higher in smaller pores. This is clearly evident for 10 Å pore. However, at high pressures larger pores favour the adsorption. This trend is in line with the results obtained for methane in carboneous material by Cao et al. [52] and Keffer et al. [53]. The amount of adsorption at a given moderate or high pressure increases with increasing pore size due to the fact that increasing pore size favours the structured layering at the surface of the adsorbent. The isotherms generated in this work are Type-1 and fit the Langmuir isotherm extremely well. The Langmuir fitting parameters are tabulated in Table 3. The maximum amount

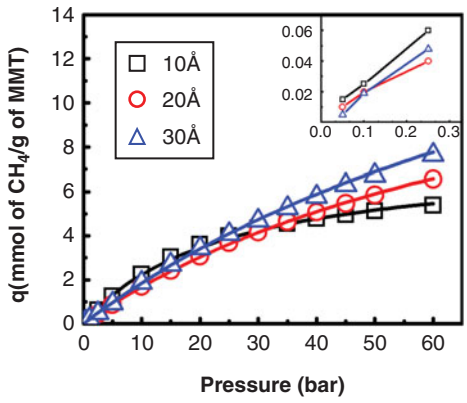

Figure 1. (Colour online) The adsorption isotherm of methane in MMT with pore size of 10 Å, 20 Å and 30 Å. The solid lines represent the fit of Langmuir isotherm. The inset presents the isotherm data for 0.1–0.3 bar.

of gas adsorbed q_m significantly increases with increase in the pore size. For example, for methane, q_m increases by twofold and threefold with increase in the pore size from 10 Å to 20 Å and 30 Å, respectively. Figure 2 presents typical snapshots for different pore sizes in order to better understand the adsorbed state of methane molecules inside the pores. It is evident from the figure that molecules tend to adsorb at the walls of the pore due to stronger fluid–wall interaction strength. As seen in Figure 2(a), for 10 Å pore, methane molecules are densely packed in two molecular layers. The increase in the pore size affects the arrangement of the molecules, which now also tends to access the region away from the surface. This reduces the overall compactness of the particle at the surface, which is clearly visible in Figure 2(b) and (c).

The layering seen in Figure 2 is clearly reflected in the density profile as shown in Figure 3(a), for a pore width of 10 Å. The increase in the pressure increases the density of the contact layer. The density at the centre of the pore, though significantly less, increases with increasing pressure. The behaviour is more or less similar at higher pore width as seen in Figure 3(b) and (c), for 20 and 30 Å, respectively. However, at a given pressure the contact layer density decreases with increase in the pore size, which is in line with the molecular configuration observed in Figure 2. In particular, the density of the contact layer in 10 Å pore is significantly higher than that in 20 and 30 Å pores. In case

Table 3. Fitting parameters of methane isotherms in Langmuir equation.

Pore size (Å)	q_m (mmol/g)	K (bar^{-1})
10	7.704	0.0407
20	15.974	0.0117
30	21.692	0.0093

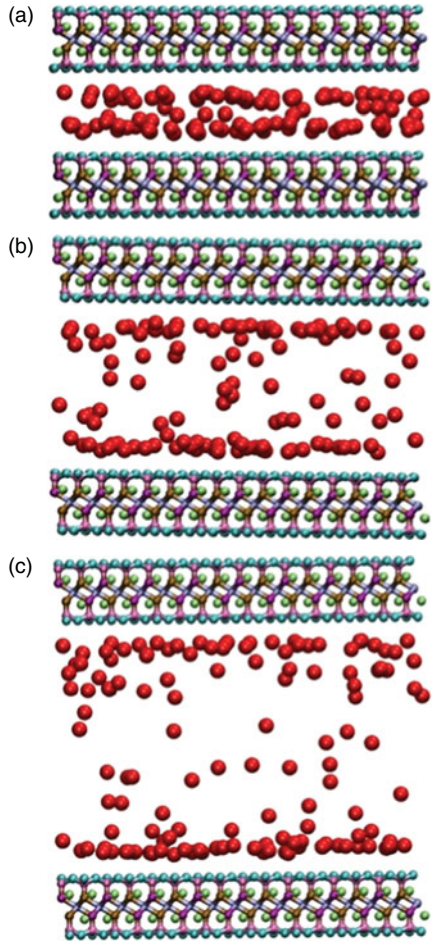

Figure 2. (Colour online) The snapshot of final configuration of methane molecules at 40 bar in MMT with pore size of (a) 10 Å, (b) 20 Å and (c) 30 Å.

of larger pores as shown in Figure 3(b) and (c), the density at the centre of the pore is significantly low, and remains constant for a large range of the pore width. The constant density region indicates the region where adsorbate molecules can freely move due to the negligible surface effect. As the pore size increases, the density in the middle of the pore (constant density region) also increases. The density profiles show that, for all pore sizes, methane forms a single layer at the surface, within the pressure range considered in this work.

Now we turn our attention to the adsorption of ethane molecules in the clay pores, as shown in Figure 4, for different pore sizes. Similar to the behaviour seen for methane, the amount of ethane adsorption at lower pressure (<10 bar) is relatively more in 10 Å than in larger pores. It should be noted that the range of pressure, where the aforementioned effect is observed, is reduced compared with that seen for methane. At higher pressure, larger pores yielded more adsorption, similar to the behaviour seen for the case of methane. The adsorption

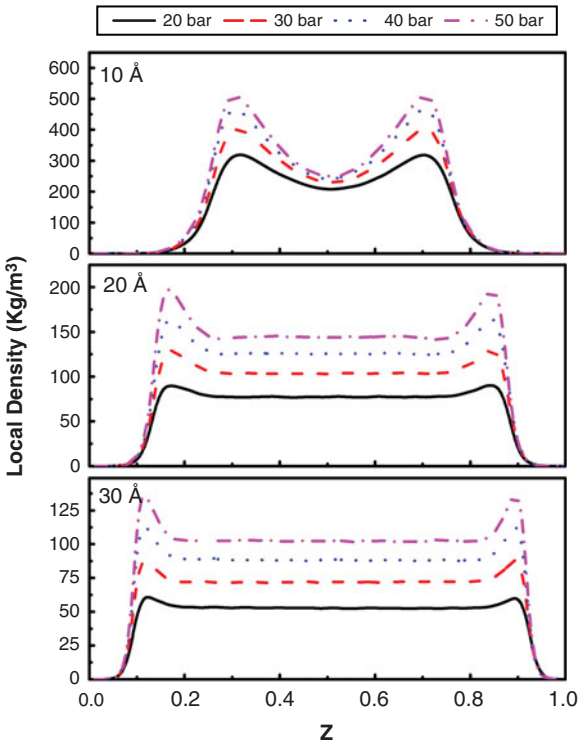

Figure 3. (Colour online) The density distribution of methane at bulk pressure of 20, 30, 40 and 50 bar in MMT with pore size of (a) 10 Å, (b) 20 Å and (c) 30 Å.

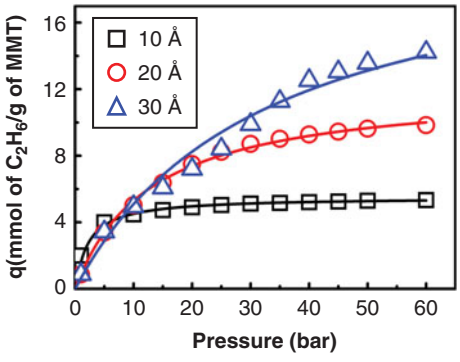

Figure 4. (Colour online) The adsorption isotherm of ethane in MMT with pore size of 10, 20 and 30 Å. The solid lines represent the fit of Langmuir isotherm.

data were fitted using the Langmuir isotherm equation, and the parameters are tabulatedd in Table 4. The behaviour of the maximum adsoption value is akin to that seen for methane. However, the maximum amount of adsorption for ethane is lower for 10 Å pore size. Nevertheless, the jump in the adsorption is significantly larger (fourfold) when pore size is increased to 30 Å. Typical snapshots of ethane molecules in 10 , 20 and 30 Å interlayer distances of MMT are shown in Figure 5. It is evident from the

Table 4. Fitting parameters of ethane isotherm in Langmuir equation.

Pore size (Å)	q_m (mmol/g)	K (bar^{-1})
10	5.504	0.456
20	12.151	0.0777
30	21.645	0.0308

adsorption isotherms of methane and ethane adsorption that, for a given pore size and pressure, the amount of ethane adsorbed is more than that of methane adsorbed on MMT surface. For small pores, 10 Å, a single layer of ethane molecules forms near the MMT surface as seen in Figure 5(a), akin to the behaviour seen for methane. The density profiles of ethane in 10 Å interlayer distance of MMT at different pressures are shown in Figure 6(a). The two density peaks in the figure confirm the formation of a single ethane layer at the wall. It also shows that the density profile of ethane is not much sensitive beyond 20 bar, indicative of saturation which is also evident from

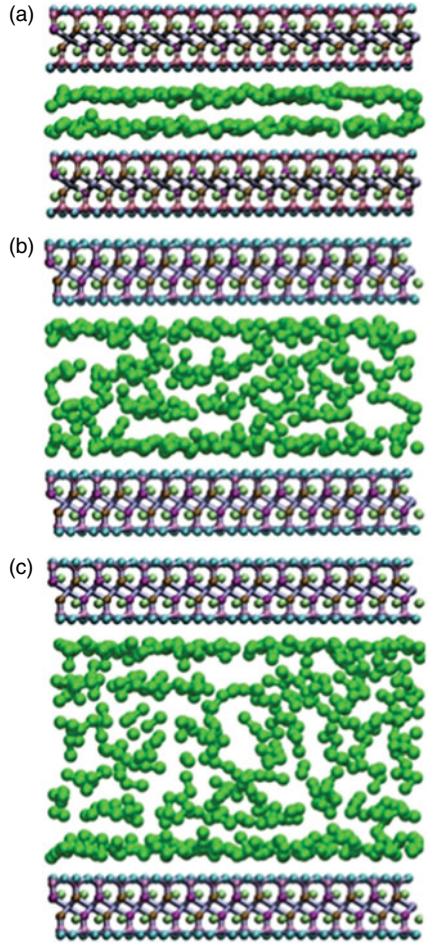

Figure 5. (Colour online) The snapshot of final configuration of ethane molecules at 40 bar in MMT with pore size of (a) 10 Å, (b) 20 Å and (c) 30 Å.

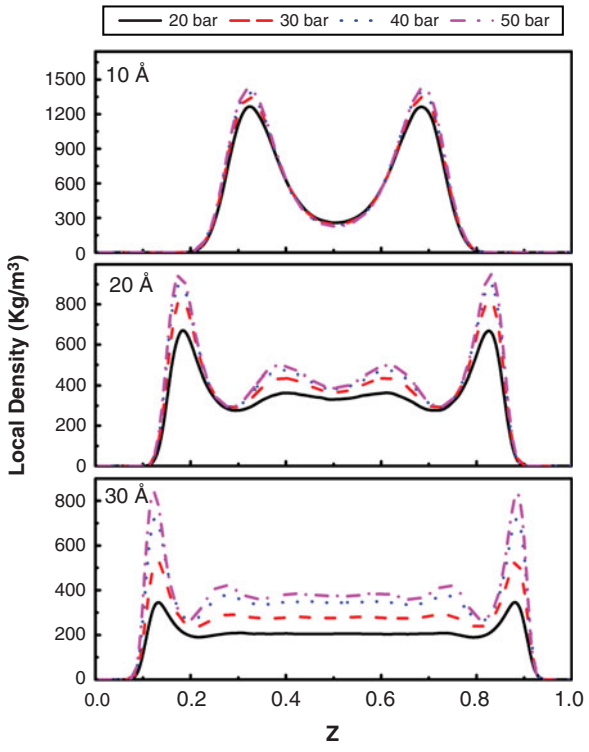

Figure 6. (Colour online) The density distribution of ethane at bulk pressure of 20, 30, 40 and 50 bar in MMT with pore size of (a) 10 Å, (b) 20 Å and (c) 30 Å.

the adsorption isotherm curve (see Figure 4). This is in contrast to the behaviour seen for methane where more response to the pressure is seen, as saturation does not reach even at 60 bar for 10 Å. This is apparent from the fact that density of ethane at the surface layer is not much sensitive to the pressure as shown in Figure 6(a). For large pores, unlike methane, the ethane molecules are densely filled throughout the pore as seen in Figure 5(b) and (c). The density profile for ethane in 20 Å pore at different pressures is shown in Figure 6(b). The ethane molecules form a double layer within the 20 Å pore size for 30, 40 and 50 bars, while, for 20 bar, a weak second layer is formed. The density profiles obtained for 30 Å pore size at different pressures are shown in Figure 6(c). Similar to the case of 20 Å pore size, ethane shows double layer formation within the 30 Å pore size. However, the strong double layer formation is only seen for 40 and 50 bars. At lower pressure, 30 bar, the second layer is very weak, and in case of 20 bar, only a single layer is formed at the MMT walls.

The structural information obtained from the GCMC simulations is further used in MD simulations in order to investigate dynamical properties of methane and ethane in MMT pores. MD simulations were performed using NVT ensemble at 298.15 K temperature for 10 20, and 30 Å interlayer distances of MMT. The data obtained from MD simulations were further used to obtain the self-diffusion coefficient of adsorbates at 20, 30, 40 and 50 bars.

Table 5. Values of self-diffusion coefficients of methane and ethane in MMT with pore size of 10, 20 and 30 Å.

	Methane			Ethane		
	$D_{\|\|} \times 10^{-7}$ m^2/s			$D_{\|\|} \times 10^{-7}$ m^2/s		
Pressure (bar)	10 (Å)	20 (Å)	30 (Å)	10 (Å)	20 (Å)	30 (Å)
10	12.55	54.21	79.53	9.20	33.18	60.13
20	5.40	20.99	29.20	6.92	14.59	30.05
30	3.65	12.58	17.60	6.48	11.07	16.21
40	3.21	8.50	13.37	5.72	9.27	10.70
50	2.81	7.36	9.80	5.32	8.80	8.60
60	2.58	5.60	8.51	5.28	7.76	8.00

3.2 Dynamical properties of methane and ethane in slit pore

The self-diffusion coefficients of methane and ethane in clay pores along the pore surface, at different pressures, are tabulated in Table 5. The effect of pressure and pore size on self-diffusion coefficients of confined fluids was well studied by various workers. For instance, H_2 and CH_4 diffusion in carbon nanotubes shows increase in the adsorption and in-plane self-diffusion coefficient with increase in pore size.[54] In case of methane adsorption in shale, using experiments and modelling techniques,[18] it was shown that the self-diffusion coefficient and adsorbed amount increase with increase in pore size. Similar behaviour was also observed for methane diffusion in single-wall carbon nanotubes (SWCNTs) at sub- and super-critical conditions.[52] Recent work of Zhang et al. [55] also reports a similar behaviour of water in SWCNTs. The methane self-diffusion coefficient at different pressures in different pore sizes is shown in Figure 7(a). The self-diffusion coefficient for methane decreases significantly with pressure, particularly for lower pressure range. However, with increase in the pore size, in-plane self-diffusion coefficient increases. Akin to the case of methane, the in-plane self-diffusion coefficient of ethane decreases with increase in pressure and increases with increase in pore size as shown in Figure 7(b). All the self-diffusion coefficients for methane and ethane in different pore sizes are of the order of 10^{-6} m^2/s, which is of the same order as obtained for methane in slit-shaped graphitic pores by Cracknell et al. [56]. However, Cao and Wu [52] obtained the self-diffusion coefficient of methane of the order of 10^{-8} m^2/s, at supercritical condition, in SWCNTs of diameters 20.34, 33.9 and 40.69 Å. We also plot the bulk diffusion values in Figure 7(a) and (b), for methane and ethane, respectively. Interestingly, the in-plane diffusion coefficient for the case of confined fluid is larger than the bulk value, particularly at lower pressures. This

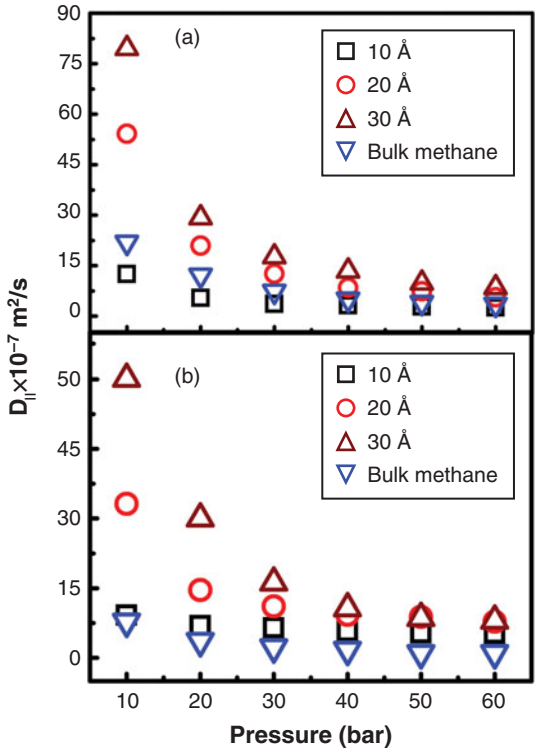

Figure 7. (Colour online) The self-diffusion coefficients of (a) methane in MMT with pore size of 10, 20 and 30 Å, (b) ethane in MMT with pore size of 10, 20 and 30 Å. The bulk diffusivity of methane and ethane is also included in the plots.

type of increase is also observed in methane diffusion in SWCNTs,[55] which is attributed to the *smoothness* of the surface and small pores.

The diffusion mechanism of adsorbate molecules in porous media can be determined by comparing the pore size with the mean free path of species.[57] The mean free path is described as:

$$\lambda = \frac{KT}{\sqrt{2}\pi d^2 P},$$

where T is the temperature, d is the collision diameter of the molecule, K is the Boltzmann constant and P is the pressure. The mean free path, calculated as per the above equation, for methane and ethane at 298.15 K and 10 bar is 67 Å and 65 Å, respectively. These values are significantly greater than the pore sizes considered here. Therefore, the diffusion is mainly controlled by Knudsen mechanism at 10 bar (or lower pressures), where molecular and pore wall collisions dominate. At a lower pore size, 10 Å, Knudsen mechanism is not expected as the pores get filled with increased density at 10 bar, as seen in Figures 2 and 5. From the kinetic theory of gases,[58] in Knudsen flow, diffusivity is directly proportional to pore diameter, i.e. the self-diffusion coefficient increases with pore diameter. The nature of diffusion coefficient at low pressure is in agreement with the prediction of the Knudsen flow. In case of high pressure, where Knudsen flow behaviour is not applicable,[52] the diffusion coefficients were found to be insensitive to the pore diameters, and as expected the behaviour is in contrast to the prediction of Knudsen flow.

3.3 *Adsorption isotherms of a binary mixture, and selectivity of species in MMT pores*

Using the single fluid results as shown above, IAST was used to predict the adsorption isotherms of methane and ethane in a mixture of 80% methane and 20% ethane using Equations (4) and (5). Furthermore, selectivity of the species was also evaluated using Equation (6). Figure 8 shows the adsorption isotherm of the binary mixture along with the fit to the Langmuir isotherm. The trend of the sorption curves is akin to that seen for pure isotherms. This is expected, as the adsorbed mixture is considered as ideal, hence the nature of the mixture isotherms and pure isotherms resembles each other. However, the amount of methane and ethane adsorbed , in mixture, is found to reduce compared with that in their pure isotherms. The percentage decrease in the adsorbed amount of methane and ethane at 40 bar is tabulated in Table 6. Interestingly, the difference of the adsorbed ethane and methane in the mixture relative to that in their pure phases decreases with increase in the pore size. However, the relative decrease is more for methane for the narrow pore size, 10 Å, which gets

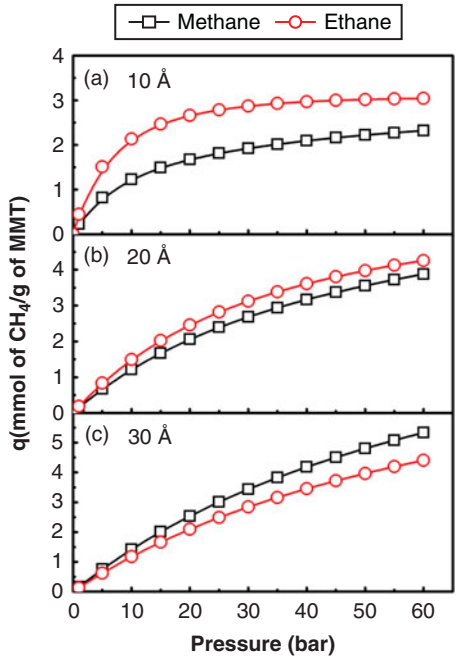

Figure 8. (Colour online) The adsorption isotherms of methane and ethane in mixture on MMT with interlayer distances of (a) 10 Å (b) 20 Å (c) 30 Å. The solid lines represent the fit of Langmuir isotherm.

Table 6. Percentage decrease in the amount of methane and ethane in mixture from their pure component adsorption amount in MMT with 10 Å, 20 Å and 30 Å pores at 40 bar.

Pore size (Å)	Methane (%)	Ethane (%)
10	56	43
20	38	61
30	28	72

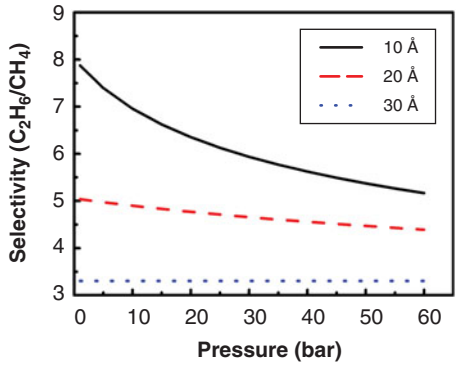

Figure 9. (Colour online) Selectivity of MMT with pore sizes of 10, 20 and 30 Å for ethane relative to methane.

suppressed for larger pores. This is apparent from the selectivity plot for ethane with respect to methane as shown in Figure 9, which presents the variation of the selectivity with the bulk pressure for different pore sizes. For 10 Å pore size, the selectivity of ethane drops sharply with increase in pressure. Further increase in pressure decreases the selectivity value, though not significantly. The selectivity of ethane drops considerably with increase in the pore size. Though the trend remains more or less similar, the effect of pressure diminishes for higher pore size, as seen for 20 Å. Further increase in the pore size to 30 Å yields adsorption isotherms of the mixture, which are independent of pressure. In summary, for the pressure range considered in this work, ethane has higher affinity towards the MMT surface, which decreases with increase in the pore size.

4. Conclusions

We have successfully generated the adsorption isotherms for pure methane and ethane in MMT pores using GCMC simulations. In addition, MD simulations were conducted to understand the structure and dynamical properties of methane and ethane in MMT pores at 298.15 K. The adsorption isotherms of pure methane and ethane follow the Langmuir isotherm. The density profiles show that methane and ethane are layered at the surface of the MMT surface, and the surface layer density increases with increase in pressure. The diffusion coefficient of methane and ethane along the pore is of the order of 10^{-6} m^2/s, which reduces with increase in pressure. The behaviour of adsorption isotherm of the mixture, evaluated using IAST, is akin to that seen for pure species. Ethane has a higher affinity for the MMT surface than methane. However, ethane selectivity decreases with increase in pore size and pressure.

Acknowledgement

The High Performance Computing (HPC) facility of Indian Institute of Technology Kanpur is gratefully acknowledged.

Funding

This work was supported by the Department of Science and Technology (DST) Government of India.

Note

1. Email: www.naturalgas.org

References

[1] Gouth F, Collell J, Galliero G, Wang J. Molecular simulation to determine key shale gas parameters, and their use in a commercial simulator for production forecasting. EAGE Annual Conference & Exhibition incorporating SPE Europec; 2013 June 10 2013.
[2] Gasparik M, Ghanizadeh A, Bertier P, Gensterblum Y, Bouw S, Krooss BM. High-pressure methane sorption isotherms of black shales from the Netherlands. Energy and Fuels. 2012;26:4995–5004.
[3] Zhang J-c, Nie H-k, Xu B, Jiang S-l, Zhang P-x, Wang Z-y. Geological condition of shale gas accumulation in sichuan basin. Natural Gas Industry. 2008;28:151–156.
[4] Montgomery SL, Jarvie DM, Bowker KA, Pollastro RM. Mississippian Barnett Shale, Fort Worth basin, north-central Texas: gas-shale play with multi-trillion cubic foot potential. AAPG Bull. 2005;89:155–175.
[5] Trikkel A, Kuusik R, Maljukova N. Distribution of organic and inorganic ingredients in Estonian oil shale semicoke. Oil Shale. 2004;21:227–235.
[6] Vandenbroucke M. Kerogen: from types to models of chemical structure. Oil Gas Sci Technol – Rev IFP. 2003;58:243–269.
[7] Vandenbrouckea M, Largeaub C. Kerogen origin, evolution and structure. Org Geochem. 2007;38:719–833.
[8] Ross DJK, Bustin RM. Characterizing the shale gas resource potential of Devonian–Mississippian strata in the Western Canada sedimentary basin: application of an integrated formation evaluation. AAPG Bull. 2008;92:87–125.
[9] Ross DJK, Bustin RM. The importance of shale composition and pore structure upon gas storage potential of shale gas reservoirs. Mar Pet Geol. 2009;26:916–927.
[10] Wenigera P, Kalkreuthb W, Buschc A, Krooss BM. High-pressure methane and carbon dioxide sorption on coal and shale samples from the Paraná Basin, Brazil. Int J Coal Geol. 2010;84:190–205.
[11] Lu X-C, Li F-C, Watson AT. Adsorption Studies of natural gas storage in Devonian shales. SPE Form Eval. 1995;10:109–113.
[12] Schettler PD Jr., Parmely CR. Contributions to total storage capacity in Devonian shales. SPE Eastern Regional Meeting; 991/1/1/; SPE 1991.
[13] Busch A, Alles S, Gensterblum Y, Prinz D, Dewhurst DN, Raven MD, Stanjek H, Krooss BM. Carbon dioxide storage potential of shales. Int J Greenhouse Gas Control. 2008;2:297–308.
[14] Wang C-C, Juang L-C, Lee C-K, Hsu T-C, Lee J-F, Chao H-P. Effects of exchanged surfactant cations on the pore structure and adsorption characteristics of montmorillonite. Journal of Colloid and Interface Science. 2004;280:27–35.

[15] Ji L, Zhang T, Milliken KL, Qu J, Zhang X. Experimental investigation of main controls to methane adsorption in clay-rich rocks. Appl Geochem. 2012;27:2533–2545.
[16] Aringhieri R. Nanoporosity characteristics of some natural clay minerals and soils. Clays Clay Miner. 2004;52:700–704.
[17] Cheng A-L, Huang W-L. Selective adsorption of hydrocarbon gases on clays and organic matter. Org Geochem. 2004;35:413–423.
[18] Yuan W, Pan Z, Li X, Yang Y, Zhao C, Connell LD, Li S, He J. Experimental study and modelling of methane adsorption and diffusion in shale. Fuel. 2014;117, Part A:509–519.
[19] Skipper NT, Refson K, McConnell JDC. Computer simulation of interlayer water in 2:1 clays. J Chem Phys. 1991;94:7434–7445.
[20] Smith DE. Molecular computer simulations of the swelling properties and interlayer structure of cesium montmorillonite. Langmuir. 1998;14:5959–5967.
[21] Young DA, Smith DE. Simulations of clay mineral swelling and hydration: dependence upon interlayer ion size and charge. J Phys Chem B. 2000;104:9163–9170.
[22] Hensen EJM, Tambach TJ, Bliek A, Smit B. Adsorption isotherms of water in Li-, Na-, and K-montmorillonite by molecular simulation. J Chem Phys. 2001;115:3322–3329.
[23] Rahimi M, Singh JK, Babu DJ, Schneider JJ, Plathe FM. Understanding carbon dioxide adsorption in carbon nanotube arrays: molecular simulation and adsorption measurements. J Phys Chem C. 2013;117:13492–13501.
[24] Samios S, Stubos AK, Kanellopoulos NK, Cracknell RF, Papadopoulos GK, Nicholson D. Determination of micropore size distribution from grand canonical Monte Carlo simulations and experimental CO_2 isotherm data. Langmuir. 1997;13:2795–2802.
[25] Vishnyakov A, Ravikovitch PI, Neimark AV. Molecular level models for CO_2 sorption in nanopores. Langmuir. 1999;15:8736–8742.
[26] Heuchel M, Davies GM, Buss E, Seaton NA. Adsorption of carbon dioxide and methane and their mixtures on an activated carbon: simulation and experiment. Langmuir. 1999;15:8695–8705.
[27] Bhatia SK, Tran K, Nguyen TX, Nicholson D. High-pressure adsorption capacity and structure of CO_2 in carbon slit pores: theory and simulation. Langmuir. 2004;20:9612–9620.
[28] Yang X, Zhang C. Structure and diffusion behavior of dense carbon dioxide fluid in clay-like slit pores by molecular dynamics simulation. Chem Phys Lett. 2005;407:427–432.
[29] Liu Y, Wilcox J. Molecular simulation of CO_2 adsorption in micro- and mesoporous carbons with surface heterogeneity. Int J Coal Geol. 2012;104:83–95.
[30] Tenney CM, Lastoskie CM. Molecular simulation of carbon dioxide adsorption in chemically and structurally heterogeneous porous carbons. Environ Prog. 2006;25:343–354.
[31] Liu Y, Wilcox J. Molecular simulation studies of CO_2 adsorption by carbon model compounds for carbon capture and sequestration applications. Environ Sci Technol. 2012;47:95–101.
[32] Furmaniak S, Terzyk AP, Gauden PA, Harris PJF, Kowalczyk P. Can carbon surface oxidation shift the pore size distribution curve calculated from Ar, N_2 and CO_2 adsorption isotherms? Simulation results for a realistic carbon model. J Phys: Condens Matter. 2009;21:315005–315014.
[33] Botan A, Rotenberg B, Marry V, Turq P, Noetinger B. Carbon dioxide in montmorillonite clay hydrates: thermodynamics, structure, and transport from molecular simulation. J Phys Chem C. 2010;114:14962–14969.
[34] Cygan RT, Romanov VN, Myshakin EM. Molecular simulation of carbon dioxide capture by montmorillonite using an accurate and flexible force field. J Phys Chem C. 2012;116:13079–13091.
[35] Allen MP, Tildesley DJ. Computer simulation of liquids. Oxford: Clarendon Press; 1987.
[36] Frenkel D, Smit B. Understanding molecular simulation: from algorithms to applications. 2nd ed. London: Academic Press; 2002.
[37] Marry V, Turq P, Cartailler T, Levesque D. Microscopic simulation of structure and dynamics of water and counterions in a monohydrated montmorillonite. J Chem Phys. 2002;117:3454–3463.
[38] Sposito G, Skipper NT, Sutton R, Park S-h, Soper AK, Greathouse JA. Surface geochemistry of the clay minerals. Proc Natl Acad Sci. 1999;96:3358–3364.
[39] Chávez-Páez M, Van Workum K, de Pablo L, de Pablo JJ. Monte Carlo simulations of Wyoming sodium montmorillonite hydrates. J Chem Phys. 2001;114:1405–1413.
[40] Skipper NT, Fang-Ru Chou C, Sposito G. Monte Carlo simulation of interlayer molecular structure in swelling clay minerals. 1. Methodology. Clays Clay Miner. 1995;43:285–293.
[41] Chang F-RC, Skipper NT, Sposito G. Computer simulation of interlayer molecular structure in sodium montmorillonite hydrates. Langmuir. 1995;11:2734–2741.
[42] Chang F-RC, Skipper NT, Sposito G. Monte Carlo and molecular dynamics simulations of interfacial structure in lithium-montmorillonite hydrates. Langmuir. 1997;13:2074–2082.
[43] de Pablo L, Chávez ML, de Pablo JJ. Stability of Na-, K-, and Ca-montmorillonite at high temperatures and pressures: a Monte Carlo simulation. Langmuir. 2005;21:10874–10884.
[44] Jorgensen WL, Madura JD, Swenson CJ. Optimized intermolecular potential functions for liquid hydrocarbons. J Am Chem Soc. 1984;106:6638–6646.
[45] Martin MG, Siepmann JI. Transferable potentials for phase equilibria. 1. United-atom description of *n*-alkanes. J Phys Chem B. 1998;102:2569–2577.
[46] Singh SK, Sinha A, Deo G, Singh JK. Vapor–liquid phase coexistence, critical properties, and surface tension of confined alkanes. J Phys Chem C. 2009;113:7170–7180.
[47] Mayo SL, Olafson BD, Goddard WA. DREIDING: a generic force field for molecular simulations. J Phys Chem. 1990;94: 8897–8909.
[48] Plimpton S. Fast parallel algorithms for short-range molecular dynamics. J Comput Phys. 1995;117:1–19.
[49] Myers AL, Prausnitz JM. Thermodynamics of mixed-gas adsorption. AIChE J. 1965;11:121–127.
[50] LeVan MD, Vermeulen T. Binary Langmuir and Freundlich isotherms for ideal adsorbed solutions. J Phys Chem. 1981;85:3247–3250.
[51] Myers AL. Equation of state for adsorption of gases and their mixtures in porous materials. Adsorption. 2003;9:9–16.
[52] Cao D, Wu J. Self-diffusion of methane in single-walled carbon nanotubes at sub- and supercritical conditions. Langmuir. 2004;20:3759–3765.
[53] Keffer D, Davis HT, MCCOrmick AV. The effect of nanopore shape on the structure and isotherms of adsorbed fluids. Adsorption. 1996;2:9–12.
[54] Skoulidas AI, Ackerman DM, Johnson JK, Sholl DS. Rapid transport of gases in carbon nanotubes. Phys Rev Lett. 2002;89:185901.
[55] Zheng Y-g, Ye H-f, Zhang Z-q, Zhang H-w. Water diffusion inside carbon nanotubes: mutual effects of surface and confinement. Phys Chem Chem Phys.14:964–971.
[56] Cracknell RF, Nicholson D, Gubbins KE. Molecular dynamics study of the self-diffusion of supercritical methane in slit-shaped graphitic micropores. J Chem Soc, Faraday Trans. 1995;91: 1377–1383.
[57] Do DD. Adsorption analysis: equilibria and kinetics. 1st ed. London: Imperial College Press; 1998.
[58] Welty J, Wicks CE, Rorrer GL, Wilson RE. Fundamentals of momentum, heat and mass transfer. 5th ed. Hobboken (NJ): John Wiley and Sons; 2008.
[59] Keith AB, Peter EK. Compositional variety complicate processing plans for US shale gas. Oil Gas J. 2009;107:50–55.